Journal of Zhejiang University-SCIENCE A (Applied Physics & Engineering)
ISSN 1673-565X (Print); ISSN 1862-1775 (Online)
www.jzus.zju.edu.cn; www.springerlink.com
E-mail: jzus@zju.edu.cn

Viscoelastic deformation behavior of cement and emulsified asphalt mortar in China railway track system I prefabricated slab track*

Juan-juan REN[†1,2], Hao-lan LI[1,2], Xiao-pei CAI[†‡3], Shi-jie DENG[1,2], Ji WANG[1,2], Wei DU[1,2]

[1]*MOE Key Laboratory of High-speed Railway Engineering, Southwest Jiaotong University, Chengdu 610031, China*

[2]*School of Civil Engineering, Southwest Jiaotong University, Chengdu 610031, China*

[3]*School of Civil Engineering, Beijing Jiaotong University, Beijing 100044, China*

[†]E-mail: renjuanjuan1983@hotmail.com; xpcai@bjtu.edu.cn

Received Oct. 19, 2019; Revision accepted Mar. 16, 2020; Crosschecked Mar. 24, 2020

Abstract: Under repeated train-induced loads, cement and emulsified asphalt mortar (CA mortar) as a viscoelastic material has a time-dependent deformation, part of which is irreversible. This could lead to debonding between the mortar layer and the track slab. Based on the theory of viscoelasticity and the analytical method of the time hardening law (THL), the viscoelastic deformation behavior of CA mortar was studied. Using ABAQUS, we established a solid model of China railway track system (CRTS) I prefabricated slab track, with CA mortar at different initial Young's moduli under cyclic loading corresponding to the influence of actual train loads. The results reveal that the fitted parameters of the THL for CA mortar are suitable for describing its viscoelastic deformation. As the initial Young's modulus increases, the strain difference before and after cyclic loading gradually decreases, and the displacement difference increases from 0.2 mm to 0.6 mm. The deformation mainly occurs at the end of a mortar layer with longitudinal distribution of about 2.5 times the fasteners' spacing. It follows that the viscoelastic performance of CA mortar is one of the most important reasons that cause debonding underneath the track slab. Therefore, we suggest that the adverse effects of viscoelastic behavior of CA mortar should be considered when researching such deformation and damage.

Key words: China railway track system (CRTS) I prefabricated slab track; Cement and emulsified asphalt mortar (CA mortar); Initial Young's modulus; Viscoelastic deformation; Time hardening law (THL)

https://doi.org/10.1631/jzus.A1900525 **CLC number:** U213

1 Introduction

With its smoothness, stability, reliability, easy maintenance, and absence of flying ballast, ballastless track has gained worldwide recognition. It is widely used in high-speed railway projects and has delivered great technical and economic benefits. As of the end of 2019, China's high-speed railways were over 35000 km in total length, and ballastless track had been adopted in over 80% of that. Among all the types of ballastless track, the China railway track system (CRTS) I prefabricated slab track, with a total length of 2700 km in service, is one of the most popular ballastless tracks in China for its low height, light weight, ease of manufacture, and low cost.

The CRTS I prefabricated slab track was a structure technically innovated from the Japanese Shinkansen slab track. As illustrated in Fig. 1, the track consists of rails, fasteners, track slabs, a layer of cement and emulsified asphalt mortar (CA mortar), concrete base, and concrete mandrel. When paved on a cast-in-place reinforced concrete base, the track slab can be adjusted by means of the CA mortar and constrained by the concrete mandrel. Resinous materials are inserted between the concrete mandrel and the

‡ Corresponding author

* Project supported by the National Natural Science Foundation of China (No. 51578472)

ORCID: Juan-juan REN, https://orcid.org/0000-0001-9500-452X; Xiao-pei CAI, https://orcid.org/0000-0003-4592-4525

track slab which is manufactured by post-tensioning. Prefabricated slabs of the CRTS I track are not longitudinally connected, and there is no lateral stopper.

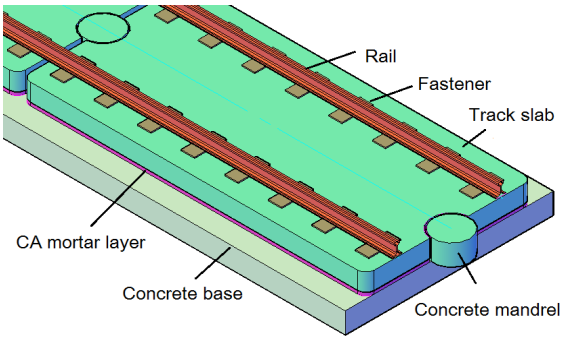

(a)

(b)

Fig. 1 CRTS I prefabricated slab track: (a) diagrammatic sketch; (b) site picture

Due to train loads, temperature changes, and other environmental factors during operation, the CRTS I prefabricated slab track inevitably becomes diseased and damaged. Suining–Chongqing railway in China was once operated as a shared passenger-freight line of ballastless track, and its design speeds of passenger and freight trains are 200 km/h and 120 km/h, respectively. In 2016, we conducted a field investigation in this railway, and found that the debonding between the CA mortar layer and track slab (Fig. 2) was one of the primary damages for the CRTS I prefabricated slab track. Some researchers (Xiang et al., 2009; Ren et al., 2014, 2017, 2020; Liu et al., 2016; Zhang et al., 2019) also discovered that the debonding had an adverse impact on track's force and deformation. For example, non-uniform interlaminar contact may cause stress concentration in local areas under loading, followed by accelerating micro-crack growth in the CA mortar which will reduce fatigue life.

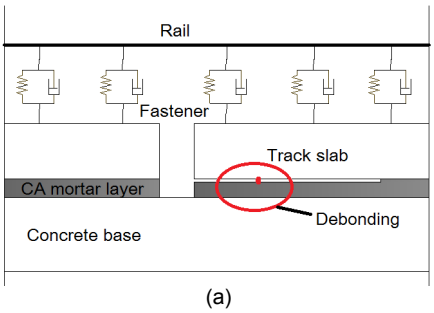

(a)

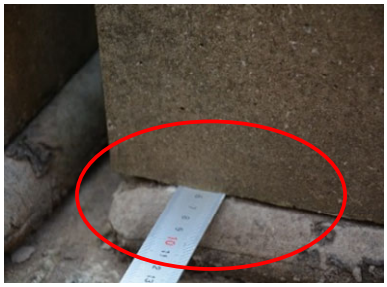

(b)

Fig. 2 Debonding between the CA mortar layer and track slab: (a) diagrammatic sketch; (b) site picture

CA mortar is a new organic-inorganic composite material composed of cement, emulsified asphalt, sand, and various admixtures. It is poured into a bag (or directly without a bag) between the track slab and the concrete base with a thickness of about 50 mm, and then formed by cement hydration and emulsified asphalt cementation (Harada, 1974, 1976; Harada et al., 1983; Ren et al., 2019). CA mortar exhibits viscoelastic properties, such as time-dependent strain, mainly contributed by emulsified asphalt, a typical kind of viscoelastic material. When subjected to external forces, the mortar deforms chronically rather than immediately, and finally reaches the maximum deformation, partly irreversible. After long-term exposure to train-induced repeated loads, the irreversible deformation of CA mortar accumulates, which may contribute to the debonding between the CA mortar layer and track slab. This draws our attention to carry out a study.

Previous laboratory tests on fatigue, strength, temperature susceptibility, and stress-strain curve have revealed that cement-asphalt emulsion composite possesses most of the characteristics of both cement and asphalt (Li et al., 1998). Also, the composition and

proportioning of cement and asphalt play a significant role in the viscoelastic behavior of CA mortar (Wang, 2008; Rutherford et al., 2014). The key parameters for its viscoelastic constitutive model, the Burgers model, were gained through curve fitting with experimental data (Liu, 2016). In addition, Zhu et al. (2014) studied the damage development of CA mortar based on the theory of viscoelasticity through numerical simulation under dynamic train loads.

The performance of CA mortar depends heavily on emulsified asphalt (Kim and Little, 2004). Hence, the studies on viscoelasticity of asphalt mixture also apply to the study of CA mortar. Monismith and Secor (1962) presented that the Burgers model could well describe the viscoelastic characteristics of asphalt concrete. Then it was employed to reliably predict the material creep response, dynamic modulus, and phase angle of mixtures with asphalt (Arabani and Kamboozia, 2013; Feng et al., 2016). Through laboratory tests, it was also pointed out that the asphalt concrete has a linear or non-linear response affected by stress level and history (Drescher et al., 1993). Temperature, frequency, and amplitude of loading are all important factors for its deformation (Judycki, 1992; Zhang et al., 1997a, 1997b; Gudmarsson et al., 2014). Specially, viscoelastic damage models of asphalt concrete were proposed to account for its rate-dependent damage growth (Park et al., 1996; Lee and Kim, 1998; Lee et al., 2000). According to the literature review, the existing studies mostly focus on the parametric analysis of viscoelastic models and the material mechanical tests. However, the exploration in the viscoelastic deformation law of CA mortar under actual train loads is little.

This paper is devoted to the viscoelastic deformation analysis of CA mortar by establishing finite element model considering the influence of actual train loads. In the model, stress and time as variables are used to calculate the deformation of the mortar. That is because the stress of CA mortar differs with time and in different locations, and constitutive models of viscoelasticity under fixed loading conditions may not be applicable in such a case. In the next sections, the viscoelastic parameters of mortar were fitted by virtue of the theory of viscoelasticity and analytical method of time hardening law (THL). Additionally, the model of CRTS I prefabricated slab track was built through ABAQUS in an effort to study the viscoelastic deformation behavior of CA mortar with different initial Young's moduli.

2 Theory of viscoelasticity

Viscoelasticity is the property of materials that exhibit both viscous and elastic characteristics when undergoing deformation (Meyers and Chawla, 2009). Unlike purely elastic materials, viscoelastic materials are rate-dependent, and the strain-time curve under a constant load can be grossly divided into three stages (Betten, 2005) as indicated in Fig. 3. In the primary stage, the strain rate is relatively high, but decreases with increasing time and strain due to a process analogous to work hardening at lower temperatures. In the secondary stage, the strain rate diminishes to a minimum and becomes near constant. In the tertiary stage, the strain rate exponentially increases with time because the necking phenomenon, internal cracks, or voids decrease the effective area of the specimen.

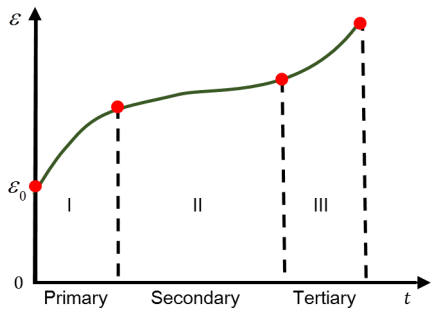

Fig. 3 Typical strain-time (ε-t) curve of viscoelastic materials under a constant load

2.1 Constitutive models of viscoelasticity

The behavior of viscoelastic materials manifests itself in transient elasticity, creep, and stress relaxation, which can be described by various constitutive models. The Burgers model gives a linearly increasing asymptote for strain under fixed loading conditions. That is, the strain increases with time, but the strain rate decreases gradually. The four-unit-five-parameter (FUFP) model (Xu, 1992), or modified Burgers model, has a nonlinearly corrected dashpot compared with the original Burgers model. The strain rate eventually becomes near zero with time and the strain tends to be constant. Both the models are well

suited for the description of the viscoelastic behavior of CA mortar (Xu et al., 2015), since they can simulate transient elastic and viscoelastic deformation in accordance with its behavior.

The Burgers model can be represented by two purely viscous dampers and two purely elastic springs connected in series, as shown in Fig. 4. The constitutive relation is expressed as

$$\varepsilon(t)=\sigma_0\left[1/E_1+t/\eta_1+(1-\mathrm{e}^{-t\tau})/E_2\right], \quad (1)$$

where σ_0 is the stress, t is the loading time, $\tau=E_2/\eta_2$, E_1 and E_2 are Young's moduli of the two springs, and η_1 and η_2 are the viscosities of the two dampers.

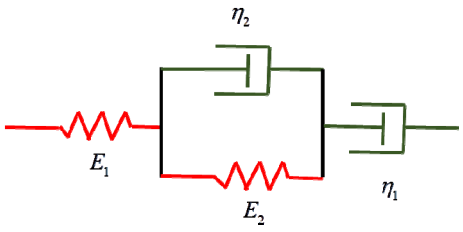

Fig. 4 Schematic representation of the Burgers model

The structure of the FUFP model is the same as that of the Burgers model. With the nonlinear correction of $\eta_1(t)=M\mathrm{e}^{Bt}$, the governing constitutive relation is

$$\varepsilon(t)=\sigma_0\left[1/E_1+(1-\mathrm{e}^{-Bt})/(MB)+(1-\mathrm{e}^{-t\tau})/E_2\right], \quad (2)$$

where M and B are both material parameters.

Xu et al. (2015) conducted laboratory tests of CA mortar in CRTS I prefabricated slab track through field sampling before train operation. When the temperature was controlled at 25 °C, the CA mortar samples with average Young's modulus of 269.58 MPa were applied to the required load and held for 60 min. The parameters of the two constitutive models are tabulated in Table 1. We can see that there is a big difference between the viscoelastic parameters of the models under different stress conditions. Therefore, it is necessary to build the model with stress as a variable to specify the viscoelastic behavior of CA mortar.

2.2 Analytical method for viscoelastic deformation

When analyzing the viscoelastic deformation, constitutive models commonly applied to CA mortar are different if subjected to varying stress. Accordingly, it is not appropriate to use models assuming fixed loading conditions to predict the behavior of CA mortar at different locations under different stresses. A model based on the THL can solve this problem by simulating the viscoelastic behavior properly.

2.2.1 Analytical method using the time hardening law

The strain of viscoelastic materials is mainly determined by loading duration t, temperature T, and stress σ, and can be expressed by

$$\varepsilon_\mathrm{c}=F(\sigma,t,T)=F_1(\sigma)F_2(t)F_3(T). \quad (3)$$

Given that the temperature is constant, the expression can be simplified as a function of time and stress. According to the Norton-Bailey law (Betten, 2005), the strain in the primary stage can be expressed as

$$\varepsilon_\mathrm{c}=F(\sigma,t)=\frac{A}{m+1}\sigma^n t^{m+1}, \quad (4)$$

where ε_c is the viscous strain except for the elastic part, σ is the equivalent stress, t is the total time, and A, m, and n are temperature dependent material constants,

Table 1 Parameters of constitutive models for CA mortar

Stress, σ_0 (MPa)	Burgers model				FUFP model				
	E_1 (MPa)	η_1 ($\times10^5$ MPa·s)	E_2 (MPa)	η_2 ($\times10^4$ MPa·s)	E_1 (MPa)	E_2 (MPa)	η_2 ($\times10^3$ MPa·s)	M ($\times10^5$ MPa·s)	B ($\times10^{-3}$ s^{-1})
0.05	31.957	9.289	163.123	1.782	33.07	201.07	6.939	2.003	0.87
0.10	33.326	13.680	172.126	1.958	35.49	204.15	3.891	1.209	1.87
0.30	58.862	13.295	168.315	1.638	62.74	204.31	6.510	1.918	1.21
0.50	84.549	16.691	215.809	2.090	90.38	275.90	9.370	2.281	1.25

which are power law multiplier, time order, and equal stress order, respectively. If the stress σ is assumed to be constant, the strain rate is given by

$$\frac{\mathrm{d}\varepsilon_c}{\mathrm{d}t} = A\sigma^n t^m. \tag{5}$$

The strain rate equation contains stress and time as variables and is therefore called the time hardening law (THL), and is used to describe the deformation behavior of viscoelastic materials.

2.2.2 Parameters of the time hardening law for CA mortar

Since the stresses in CA mortar at different positions are different under train loads, Eq. (4) is adopted in this research to predict its deformation behavior. The input parameters are A, m, and n. Using the parameters in Table 1, we performed curve fitting to obtain the three parameters of the THL, as listed in Table 2. Corresponding to the Burgers model, the mean values of the parameters are A=3.677×10^{-8}, m=−0.7675, and n=0.5935, while corresponding to the FUFP model, they are A=6.131×10^{-8}, m=−0.8762, and n=0.6085.

In order to verify the rationality of the parameters obtained above, we established a simple solid model of size of 1 m×1 m×2 m. In the model, an area load of 0.1 MPa was applied to simulate the effect of a train load, because the compressive stress in CA mortar is about 0.1 MPa when a train is running through (Xu et al., 2011). Then comparison of the strain results between models is presented in Fig. 5.

The results show that the overall trend of deformation from constitutive models is consistent with that from models based on THL, but THL-based models deform slightly less than constitutive models in the early period. The maximum percentage difference between the Burgers model and the THL-based Burgers model is −3.97%, while it is −4.57% between the FUFP model and the THL-based FUFP model. However, the differences both decrease with time. Furthermore, the deformations of the THL-based Burgers model are slightly greater than those of the THL-based FUFP model, and the deformation curves of the Burgers model and the FUFP model show an intersection. The main reason for such a difference may be that the mean fitted parameters of THL comprehensively take into account various stress conditions that deviate from the single condition of 0.1 MPa. To sum up, the fitted parameters of the THL are suitable for describing the viscoelastic deformation of CA mortar.

3 Slab track modelling with time hardening law

3.1 Solid model of CRTS I prefabricated slab track

To characterize the viscoelastic deformation of CA mortar, we established a solid model of CRTS I

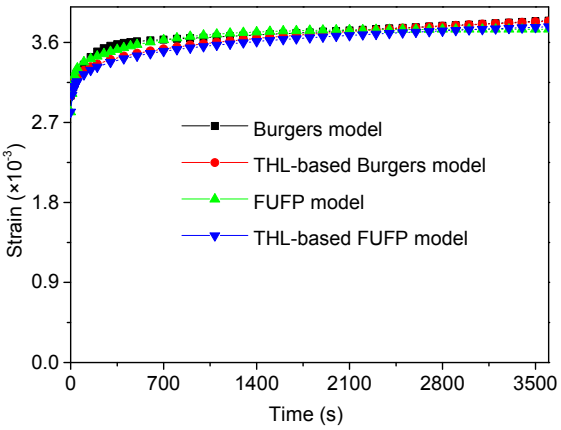

Fig. 5 Strain comparison of CA mortar between models

Table 2 Parameters of the THL for CA mortar

Stress, σ (×10^6 Pa)	Burgers model			FUFP model		
	A (×10^{-8})	m	n	A (×10^{-8})	m	n
0.05	3.549	−0.7374	0.5670	4.230	−0.8274	0.6082
0.10	3.613	−0.7876	0.5908	5.815	−0.9069	0.6056
0.30	3.869	−0.7776	0.6227	8.248	−0.8943	0.6117
0.50	3.652	−0.7794	0.6240	7.772	−0.8746	0.6124
Mean	3.677	−0.7675	0.5935	6.131	−0.8762	0.6085

prefabricated slab track through ABAQUS. The parameters of the THL determined in Section 2 were used here. In the model, solid elements C3D8R were used for the simulation of rails, track slabs, CA mortar layer, and concrete base, which all had the approximate size of 0.1 m. There were 2152 elements of the CA mortar layer underneath a track slab, which included 2320 elements. Fasteners and foundation were both simulated by spring-damping elements to represent the damping effects.

The vertical damping constant of CA mortar was 34.58 N·s/m and its initial Young's moduli were designed as 100 MPa, 300 MPa, and 500 MPa, respectively. Young's modulus of CA mortar is typically 100 MPa to 500 MPa in CRTS I prefabricated slab track. In the process of real operation, the modulus is liable to change due to on-site construction and other external conditions such as train operation, temperature, and rain. It is obvious that the stress in CA mortar is different if the modulus changes. Referring to Eq. (4), the stress affects the viscoelastic deformation of CA mortar directly. Consequently, the initial Young's moduli of CA mortar were designed as 100 MPa, 300 MPa, and 500 MPa to research the viscoelastic deformation of CA mortar with different moduli. Other model parameters adopted are listed in Table 3.

As transverse and longitudinal constraints on a track slab, the concrete mandrel was simplified in modelling because its impact on the track's vertical force was too small (Liang, 2013; Xie, 2016). The rail ends were constrained in space, and a contact boundary was employed between track slab, concrete base, and CA mortar. The model did not consider the change of lateral friction force of CA mortar layer under compression and deformation because the mortar is designed mainly to bear pressure. Five track slabs were modeled to reduce boundary effects on computing results, and we chose the middle one for analysis. Figs. 6 and 7 show the mechanical schematic diagram and the finite element model of the slab track.

3.2 Cyclic loading considering the influence of actual train loads

For the simulation, necessary consideration is given to the different train loads corresponding to various speeds and axle loads of passenger or freight trains, but few studies have so far analyzed the structural deformation of slab track under actual train loads. We performed a field investigation on the Suining–Chongqing railway to obtain the vertical wheel-rail forces. The layout of measuring points is demonstrated in Fig. 8. Points 1 and 2 were located at the rail web between two adjacent slabs, and points 3 and 4 were set on the rail web in the middle of the track slab. Additionally, the track structure where these points were located was in good condition.

Table 3 Model parameters for CRTS I prefabricated slab track

Component	Parameter	Value
Rail	Young's modulus, E_r ($\times10^{11}$ N/m^2)	2.059
	Poisson's ratio, v_r	0.3
	Mass per unit length, m_r (kg/m)	60.64
Fastener	Spacing, L_f (m)	0.625
	Vertical stiffness, K_f ($\times10^7$ N/m)	6.0
	Vertical damping, C_f ($\times10^5$ N·s/m)	3.625
Track slab	Length, L_s (m)	4.93
	Width, W_s (m)	2.4
	Height, H_s (m)	0.19
	Young's modulus, E_s ($\times10^{10}$ N/m^2)	3.65
	Poisson's ratio, v_s	0.2
Concrete base	Width, W_b (m)	3.2
	Height, H_b (m)	0.3
	Young's modulus, E_b ($\times10^{10}$ N/m^2)	3.25
	Poisson's ratio, v_b	0.2
Foundation	Surface stiffness, K_l (MPa/m)	75
	Vertical damping, C_l ($\times10^5$ N·s/m)	1.0

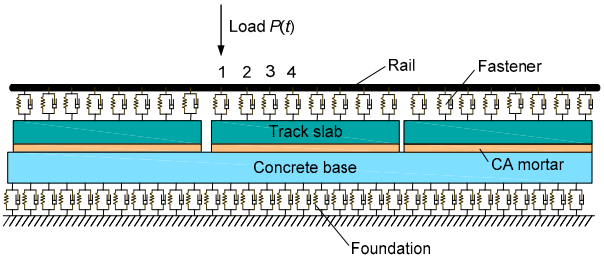

Fig. 6 Mechanical schematic diagram of CRTS I prefabricated slab track

Fig. 9 shows the site test where strain gauges were arranged in a full-bridge configuration. The actual vertical wheel-rail force when passenger and freight trains are running through can be obtained by converting the data tested after calibration.

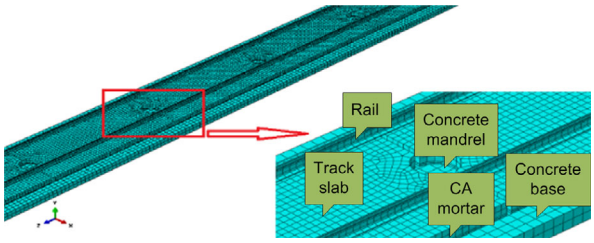

Fig. 7 Finite element model of CRTS I prefabricated slab track

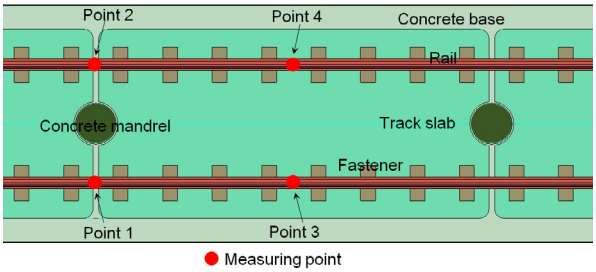

Fig. 8 Layout of measuring points for vertical wheel-rail forces

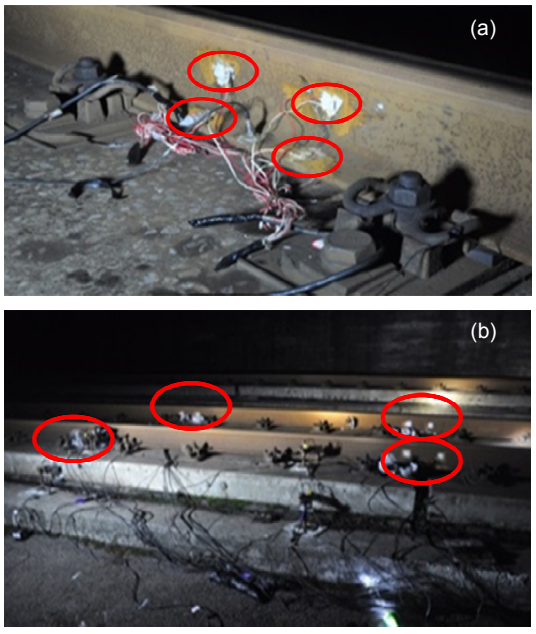

Fig. 9 Site test of the vertical wheel-rail force in the Suining–Chongqing railway: (a) strain gauges; (b) measuring points

From the test, we got data samples of 10168 for 37 passenger trains and of 10768 for 18 freight trains. The vertical wheel-rail forces under passenger and freight trains are partially plotted in Fig. 10. Through statistical analysis (Zhao, 2017), the 95% confidence interval of wheel-rail forces is between 44.46 kN and 89.88 kN with a median of 70 kN under passenger trains, while the interval is between 81.22 kN and 142.42 kN under freight trains.

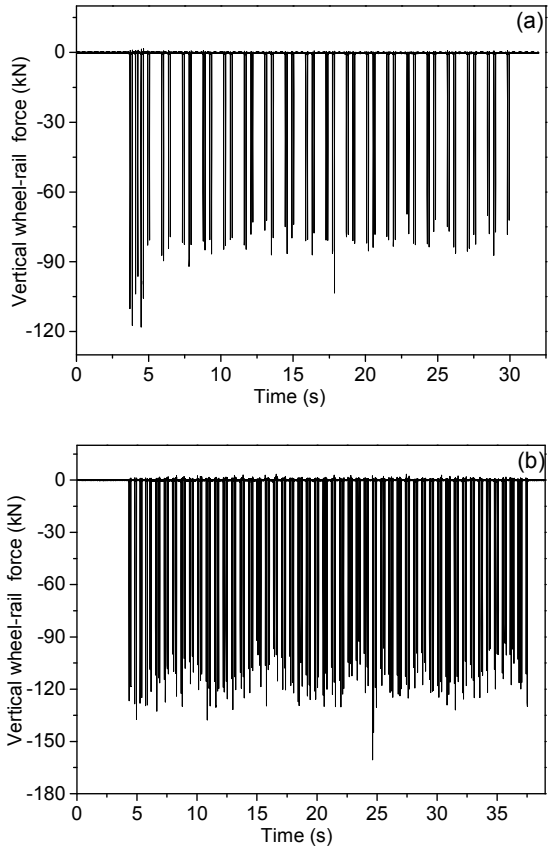

Fig. 10 Vertical wheel-rail forces measured in the site test: (a) passenger train; (b) freight train

Under the short-time influence of a running train, CA mortar deforms and then recovers to its original shape with viscosity playing a small role. Thus, it is reasonable to assume the mortar as purely elastic when analyzing the dynamic response of the track structure in such a case. Actually, CA mortar displays time-dependent deformation when track structures are subjected to repetitive train loads, so it is meaningful to study the effects of its viscoelastic performance on track structures. According to the confidence interval

above, the range of 70 kN to 150 kN was adopted in sinusoidal loading (Fig. 11). The period of the curve is 30 s which roughly equals the time for a train passing, and the loading time was 3600 s, corresponding to the test conducted by Xu et al. (2015). The slab end is where the mortar damage usually occurs (Xu et al., 2013), and the rail head at the first fastening location was selected as the loading position in the simulation (Fig. 6). Moreover, data extraction was conducted at the location.

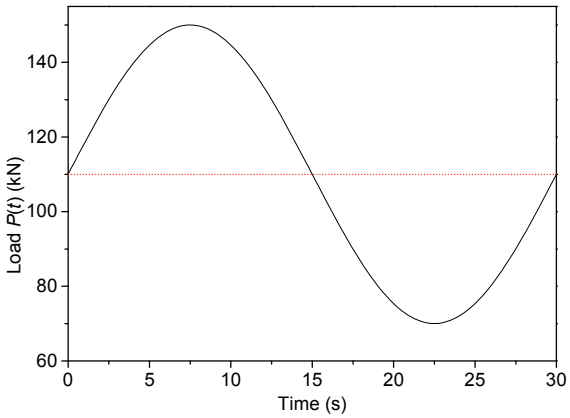

Fig. 11 One cycle of the cyclic loading curve

4 Viscoelastic deformation behavior of CA mortar under cyclic loading

4.1 Stress-strain curve of CA mortar

As for the whole cyclic loading, a similar trend of stress-strain curve applies to CA mortars with different initial Young's moduli. Figs. 12 and 13 depict respectively the stress-strain curve and the increment of trough strain with cycles of THL-based FUFP model.

From Fig. 12, we can see that with the same initial Young's modulus, cyclic loading causes not only an increase of the strain but also a decrease of the stress of CA mortar. On the assumption that the strain is constant, the stress decreases and then gradually stabilizes, indicating a decrease of Young's modulus, or cyclic softening. It is noted from Fig. 13 that when the initial Young's modulus of CA mortar varies from 100 MPa to 500 MPa, the increment of trough strain between two adjacent cycles decreases rapidly and then levels off. The larger the initial Young's modulus is, the faster the rate of decrease will be.

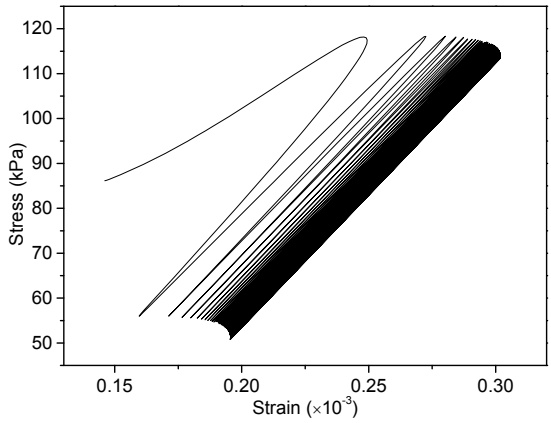

Fig. 12 Stress-strain curve of CA mortar (500 MPa)

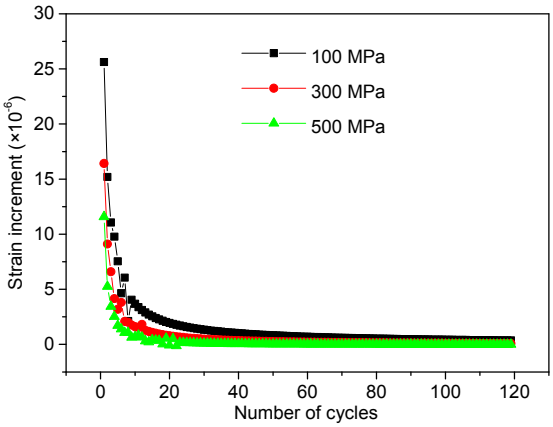

Fig. 13 Increments of trough strain of CA mortar with different initial Young's moduli

4.2 Vertical strain and displacement of CA mortar

For the viscoelastic deformation of CA mortar in THL-based models in numerical analysis, a close agreement in distribution exists for different initial Young's moduli. Fig. 14 shows the vertical strain and displacement distribution of the THL-based FUFP model after cyclic loading.

It can be seen from Fig. 14 that the vertical viscoelastic strain appears mainly at the end of the CA mortar layer and concentrates at its edge. The strain is obvious between the end of the layer and the third fastener with a longitudinal distribution equivalent to about 2.5 times the spacing of the fasteners. The vertical displacement largely distributes in the area of three fasteners at the slab end, with a longer transmission distance and a slightly wider distribution. With the same initial Young's modulus, the vertical strain and displacement of mortar of the THL-based

Burgers model are slightly larger than those of the THL-based FUFP model, but the two models have a similar deformation distribution.

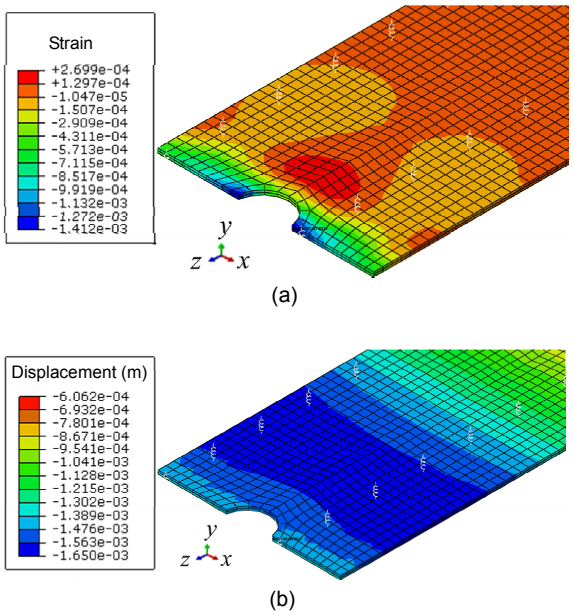

Fig. 14 Viscoelastic deformation distribution of CA mortar (the initial Young's modulus is 500 MPa): (a) vertical strain; (b) vertical displacement

Moreover, we can get the vertical strain and displacement curves of CA mortar under cyclic loading, as demonstrated in Fig. 15, where the strain and displacement of the THL-based FUFP model are plotted as functions of time.

From Fig. 15, it can be observed that during the process of cyclic loading, the viscoelastic deformation of CA mortar in each cycle has a local maximum and minimum which are greater than their counterparts in the previous cycle. In other words, the viscoelastic deformation of mortar gradually accumulates with cycles. With the same initial Young's modulus, the deformation of the THL-based Burgers model has the same tendency as that of the THL-based FUFP model. Besides, the strain increments at peak and trough of the former model are slightly larger than those of the latter. The displacement increments at the peak of the former model are slightly larger than those of the latter, while those at the trough are smaller. In general, the difference of displacement increments between the two models after cyclic loading is no greater than 0.02 mm. Therefore, we can conclude that there is a consistency in the viscoelastic deformation in the two models.

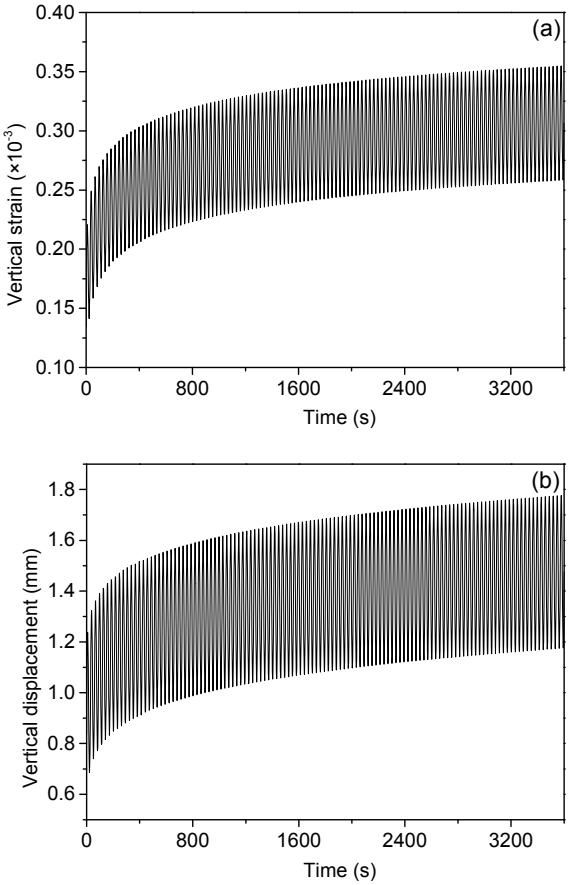

Fig. 15 Viscoelastic deformation of CA mortar (the initial Young's modulus is 500 MPa): (a) vertical strain; (b) vertical displacement

4.3 Deformation difference of CA mortar with different initial Young's moduli

Before and after cyclic loading, the peak strain and displacement of mortar with different initial Young's moduli were obtained from the THL-based Burgers model, as shown in Fig. 16.

When the initial Young's modulus of the mortar increases, its initial strain and displacement (before cyclic loading) decrease as well as the final values (after cyclic loading). The final strain is 1.635×10^{-3} with an initial Young's modulus of 100 MPa, while the value is 0.368×10^{-3} at 500 MPa, just 0.225 times of the former. Similarly, the final displacement is 2.364 mm at 100 MPa, and 1.861 mm at 500 MPa, 0.787 times of the former. The increase of the initial

Young's modulus not only leads to reduced initial and final strain, but also causes reduction of initial and final displacement as a result of the increasing stiffness of the whole track structure (Luo, 2014).

Finally, a detailed comparison of strain differences as well as displacement differences before and after cyclic loading of CA mortar is made between THL-based models, as shown in Table 4 and Fig. 17.

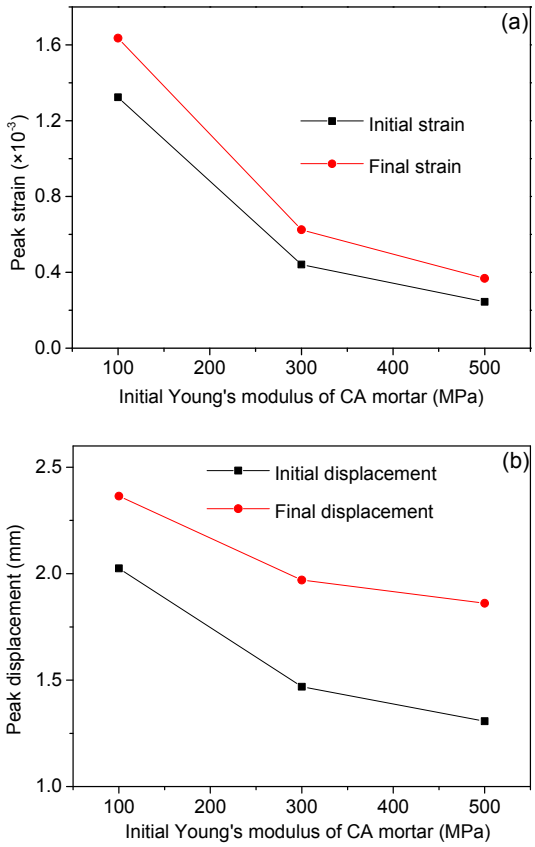

Fig. 16 Deformation of CA mortar with different initial Young's moduli before and after cyclic loading: (a) vertical strain; (b) vertical displacement

5 Conclusions

This study employed FUFP and Burgers models to simulate the viscoelastic deformation of CA mortar. The viscoelastic parameters of mortar from the THL were obtained by curve fitting, followed by rationality verification. Then, we established a solid model of CRTS I slab track with the THL, applied cyclic loads considering the influence of actual train loads on the model, and analyzed the viscoelastic deformation of mortars with different initial Young's moduli according to the numerical results. Some conclusions can be summarized as follows:

1. The parameters of the THL of CA mortar for the Burgers model, namely A, m, and n, are 3.677×10^{-8}, -0.7675, and 0.5935, respectively, and they are 6.131×10^{-8}, -0.8762, and 0.6085, respectively, for the FUFP model. It is verified that the THL-based models can well predict the viscoelastic deformation of CA mortar. Additionally, the deformation of the THL-based Burgers model is slightly larger than that of the THL-based FUFP model.

Table 4 Deformation comparison for CA mortars with different initial Young's moduli (Diff.=difference)

Initial Young's modulus (MPa)	Peak/ Trough	Initial/ Final cycle	THL-based Burgers model				THL-based FUFP model			
			Strain ($\times10^{-3}$)		Displacement (mm)		Strain ($\times10^{-3}$)		Displacement (mm)	
			Value	Diff.	Value	Diff.	Value	Diff.	Value	Diff.
100	Peak	Initial	1.323	0.312	2.025	0.339	1.288	0.297	1.988	0.320
		Final	1.635		2.364		1.585		2.308	
	Trough	Initial	0.707	0.267	1.042	0.289	0.657	0.274	0.989	0.298
		Final	0.974		1.331		0.931		1.287	
300	Peak	Initial	0.441	0.185	1.469	0.501	0.411	0.191	1.406	0.489
		Final	0.625		1.970		0.602		1.895	
	Trough	Initial	0.274	0.154	0.836	0.431	0.237	0.167	0.753	0.439
		Final	0.429		1.268		0.405		1.192	
500	Peak	Initial	0.245	0.123	1.307	0.554	0.219	0.136	1.235	0.541
		Final	0.368		1.861		0.355		1.776	
	Trough	Initial	0.172	0.099	0.780	0.472	0.141	0.117	0.685	0.491
		Final	0.271		1.252		0.258		1.176	

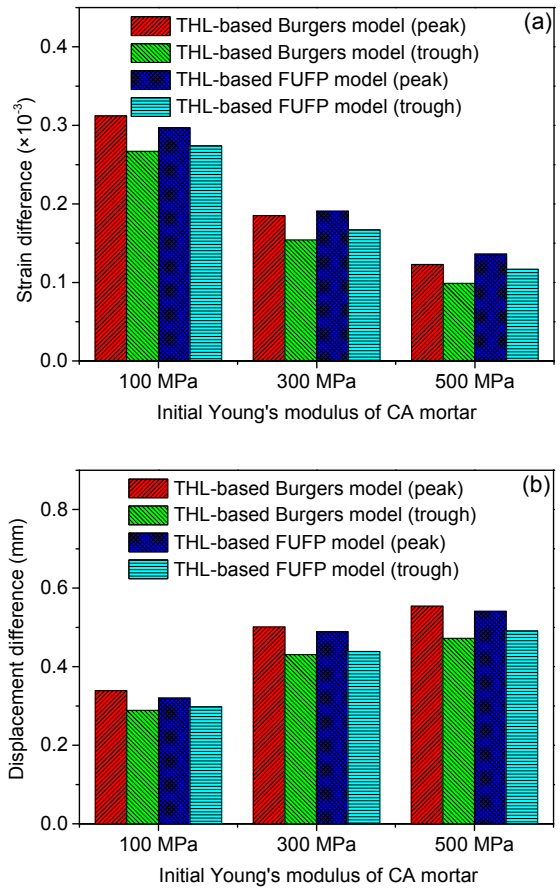

Fig. 17 Deformation differences before and after cyclic loading of CA mortars: (a) vertical strain difference; (b) vertical displacement difference

2. The stress-strain curve of CA mortar displays characteristics of cyclic softening under cyclic loading. The strain increment between two adjacent cycles decreases rapidly and tends to level off with cycles. A higher initial Young's modulus corresponds to a more rapid decrease.

3. The vertical viscoelastic strain mainly appears at the end of a CA mortar layer and concentrates at the edge, with longitudinal distribution being about 2.5 times the fasteners' spacing.

4. When the initial Young's modulus of a CA mortar increases from 100 MPa to 500 MPa, the strain decreases, so does the strain difference before and after cyclic loading. Nevertheless, the variation has little effect on the displacement of the mortar. The displacement difference before and after cyclic loading of CA mortars with different initial Young's moduli is mainly in the range of 0.2 mm to 0.6 mm, in which part of the deformation is non-elastic and irreversible.

It follows that the viscoelastic performance of CA mortar is one of the most important reasons for the debonding between the CA mortar and the track slab. Once the debonding is formed, the mortar may be squeezed and slapped by the track slab during train operation. This may lead to stress concentration, which further gives rise to cracks and fatigue damage accumulating in the mortar. Therefore, we suggest future studies consider the adverse effects of viscoelastic behavior of mortar when researching mortar deformation and damage.

Contributors

Juan-juan REN designed the research. Xiao-pei CAI processed the corresponding data. Hao-lan LI wrote the first draft of the manuscript. Shi-jie DENG, Ji WANG, and Wei DU helped to organize the manuscript. Hao-lan LI and Juan-juan REN revised and edited the final version.

Conflict of interest

Juan-juan REN, Hao-lan LI, Xiao-pei CAI, Shi-jie DENG, Ji WANG, and Wei DU declare that they have no conflict of interest.

References

Arabani M, Kamboozia N, 2013. The linear visco-elastic behaviour of glasphalt mixture under dynamic loading conditions. *Construction and Building Materials*, 41:594-601. https://doi.org/10.1016/j.conbuildmat.2012.12.023

Betten J, 2005. Creep Mechanics. Springer, Berlin, Germany, p.50-75.

Drescher A, Kim JR, Newcomb DE, 1993. Permanent deformation in asphalt concrete. *Journal of Materials in Civil Engineering*, 5(1):112-128. https://doi.org/10.1061/(asce)0899-1561(1993)5:1(112)

Feng H, Pettinari M, Stang H, 2016. Three different ways of calibrating Burger's contact model for viscoelastic model of asphalt mixtures by discrete element method. The 8th RILEM International Symposium on Testing and Characterization of Sustainable and Innovative Bituminous Materials, p.423-433. https://doi.org/10.1007/978-94-017-7342-3_34

Gudmarsson A, Ryden N, Birgisson B, 2014. Observed deviations from isotropic linear viscoelastic behavior of asphalt concrete through modal testing. *Construction and Building Materials*, 66:63-71. https://doi.org/10.1016/j.conbuildmat.2014.05.077

Harada Y, 1974. Development and utility of grout for a track structure with grout-filled ballast. *Quarterly Reports*, 15(1):25-27.

Harada Y, 1976. Development of ultrarapid-hardening cement-asphalt mortar for grouted-ballast track structure. *Quarterly Reports*, 17(1):6-11.

Harada Y, Tottori S, Itai N, et al., 1983. Development of cement-asphalt mortar for slab tracks in cold climate. *Quarterly Reports*, 24(2):62-67.

Judycki J, 1992. Non-linear viscoelastic behaviour of conventional and modified asphaltic concrete under creep. *Materials and Structures*, 25(2):95-101. https://doi.org/10.1007/BF02472462

Kim YR, Little DN, 2004. Linear viscoelastic analysis of asphalt mastics. *Journal of Materials in Civil Engineering*, 16(2):122-132. https://doi.org/10.1061/(asce)0899-1561(2004)16:2(122)

Lee HJ, Kim YR, 1998. Viscoelastic continuum damage model of asphalt concrete with healing. *Journal of Engineering Mechanics*, 124(11):1224-1232. https://doi.org/10.1061/(asce)0733-9399(1998)124:11(1224)

Lee HJ, Daniel JS, Kim YR, 2000. Continuum damage mechanics-based fatigue model of asphalt concrete. *Journal of Materials in Civil Engineering*, 12(2):105-112. https://doi.org/10.1061/(asce)0899-1561(2000)12:2(105)

Li G, Zhao Y, Pang SS, et al., 1998. Experimental study of cement-asphalt emulsion composite. *Cement and Concrete Research*, 28(5):635-641. https://doi.org/10.1016/S0008-8846(98)00038-6

Liang F, 2013. Mechanical Characteristic Research of CRTS I Slab Ballastless Track. MS Thesis, Central South University, Changsha, China (in Chinese).

Liu D, Liu YF, Ren JJ, et al., 2016. Contact loss beneath track slab caused by deteriorated cement emulsified asphalt mortar: dynamic characteristics of vehicle-slab track system and prototype experiment. *Mathematical Problems in Engineering*, 2016:3073784. https://doi.org/10.1155/2016/3073784

Liu Z, 2016. Effect of Temperature Load on CA Mortar Filling Layer of CRTS I Slab Track. PhD Thesis, Southwest Jiaotong University, Chengdu, China (in Chinese).

Luo W, 2014. CA Mortar Fatigue Damage and Its Effect on Vibration Response of Track Structure. MS Thesis, Zhejiang University of Technology, Hangzhou, China (in Chinese).

Meyers MA, Chawla KK, 2009. Mechanical Behavior of Materials. Cambridge University Press, Cambridge, UK, p.120-126.

Monismith CL, Secor KE, 1962. Viscoelastic behavior of asphalt concrete pavements. International Conference on the Structural Design of Asphalt Pavements, p.476-498.

Park SW, Kim YR, Schapery RA, 1996. A viscoelastic continuum damage model and its application to uniaxial behavior of asphalt concrete. *Mechanics of Materials*, 24(4):241-255. https://doi.org/10.1016/S0167-6636(96)00042-7

Ren JJ, Yan XB, Xu GH, et al., 2014. Effects of contact loss underneath concrete roadbed on dynamic performances of slab track-subgrade system. *Journal of Southwest Jiaotong University*, 49(6):961-966 (in Chinese). https://doi.org/10.3969/j.issn.0258-2724.2014.06.005

Ren JJ, Yang RS, Wang P, et al., 2017. Influence of contact loss underneath concrete underlayer on dynamic performance of prefabricated concrete slab track. *Proceedings of the Institution of Mechanical Engineers, Part F: Journal of Rail and Rapid Transit*, 231(3):345-358. https://doi.org/10.1177/0954409716630339

Ren JJ, Deng SJ, Wei K, et al., 2019. Mechanical property deterioration of the prefabricated concrete slab in mixed passenger and freight railway tracks. *Construction and Building Materials*, 208:622-637.

Ren JJ, Wang J, Li X, et al., 2020. Influence of cement asphalt mortar debonding on the damage distribution and mechanical responses of CRTS I prefabricated slab. *Construction and Building Materials*, 230:116995. https://doi.org/10.1016/j.conbuildmat.2019.116995

Rutherford T, Wang ZJ, Shu X, et al., 2014. Laboratory investigation into mechanical properties of cement emulsified asphalt mortar. *Construction and Building Materials*, 65:76-83. https://doi.org/10.1016/j.conbuildmat.2014.04.113

Wang T, 2008. Research and Application on CA Mortar in Ballastless Slab Track of High Speed Railway. PhD Thesis, Wuhan University of Technology, Wuhan, China (in Chinese).

Xiang J, He D, Zeng QY, 2009. Effect of cement asphalt mortar disease on dynamic performance of slab track. *Journal of Central South University (Science and Technology)*, 40(3):791-796 (in Chinese).

Xie P, 2016. Study on Fatigue Property of the CRTS I Slab Track for Mixed Passenger and Freight Railway. MS Thesis, Southwest Jiaotong University, Chengdu, China (in Chinese).

Xu H, Wang P, Xie KZ, et al., 2015. Test and model parameter analysis of cement and emulsified asphalt mortar with short-term creep property. *Journal of the China Railway Society*, 37(9):114-118 (in Chinese). https://doi.org/10.3969/j.issn.1001-8360.2015.09.016

Xu K, Zhao ZG, Ren JJ, 2013. Influence of CA mortar damage on structural forces in slab track. *Chinese Railways*, (9):68-72 (in Chinese). https://doi.org/10.3969/j.issn.1001-683X.2013.09.019

Xu QY, Li B, Zhou XL, 2011. Dynamic coefficient of slab track system on subgrade under high-speed trains. *Journal of Central South University (Science and Technology)*, 42(9):2831-2836 (in Chinese).

Xu SF, 1992. Rheological model for specifying the creep properties of asphalt and asphalt mixture with high and low temperatures. *Mechanics and Engineering*, 14(1):37-40 (in Chinese).

Zhang W, Drescher A, Newcomb DE, 1997a. Viscoelastic analysis of diametral compression of asphalt concrete. *Journal of Engineering Mechanics*, 123(6):596-603. https://doi.org/10.1061/(asce)0733-9399(1997)123:6(596)

Zhang W, Drescher A, Newcomb DE, 1997b. Viscoelastic

behavior of asphalt concrete in diametral compression. *Journal of Transportation Engineering*, 123(6):495-502. https://doi.org/10.1061/(asce)0733-947x(1997)123:6(495)

Zhang YR, Cai XP, Gao L, et al., 2019. Improvement on the mechanical properties of CA mortar and concrete composite specimens in high-speed railway by modification of interlayer bonding. *Construction and Building Materials*, 228:116758. https://doi.org/10.1016/j.conbuildmat.2019.116758

Zhao HW, 2017. The Train Load Characteristics for Mixed Passenger and Freight Railways with Ballastless Track. MS Thesis, Southwest Jiaotong University, Chengdu, China (in Chinese).

Zhu SY, Fu Q, Cai CB, et al., 2014. Damage evolution and dynamic response of cement asphalt mortar layer of slab track under vehicle dynamic load. *Science China Technological Sciences*, 57(10):1883-1894. https://doi.org/10.1007/s11431-014-5636-8

中文概要

题　目： 中国铁路轨道系统 I 型板式无砟轨道中水泥乳化沥青砂浆的粘弹性变形分析研究

目　的： 作为粘弹性材料，水泥乳化沥青（CA）砂浆的变形依赖于时间，且包含不可恢复变形，使得轨道板与 CA 砂浆层之间形成离缝，进而影响轨道的结构受力与变形。本文旨在研究 CA 砂浆在列车荷载作用下、不同初始弹性模量时的粘弹性变形规律，以期为轨道结构的维修养护提供参考。

创新点： 1. 以粘弹性理论与时间硬化率分析方法为基础，拟合得到 CA 砂浆的时间硬化率特征参数；2. 建立基于时间硬化率的中国铁路轨道系统（CRTS）I 型板式无砟轨道实体模型，成功模拟了 CA 砂浆的粘弹性变形过程。

方　法： 1. 运用 Burgers 与四单元五参数粘弹性本构方程，拟合得到 CA 砂浆的时间硬化率特征参数，并验证该参数的合理性（图 5）；2. 结合现场测试所得钢轨支点压力，统计分析得到有限元模型循环加载的幅值与周期（图 11）；3. 通过仿真模拟，得到 CA 砂浆在列车荷载作用下、不同初始弹性模量时的粘弹性变形，进而探寻 CA 砂浆的粘弹性变形规律（图 16 和 17）。

结　论： 1. 基于时间硬化率的分析模型能较好地模拟 CA 砂浆变形行为。2. 随着 CA 砂浆初始弹性模量的增大，CA 砂浆在粘弹性变形前后的应变差值逐渐减小，位移差值逐渐增大；位移差值集中于 0.2~0.6 mm，且变形敏感区域约为板端 2.5 个扣件间距。3. CA 砂浆本身粘弹性特征引起的不可恢复变形是导致 CA 砂浆层与轨道板之间形成离缝的重要原因之一；在研究 CA 砂浆变形及损伤时，建议考虑 CA 砂浆粘弹性行为及其变形特征的不利影响。

关键词： CRTS I 型板式无砟轨道；CA 砂浆；初始弹性模量；粘弹性变形；时间硬化率